Journal of ELECTRONIC MATERIALS, Vol. 43, No. 10, 2014
DOI: 10.1007/s11664-014-3214-2

Electronic Structure and Thermoelectric Properties of Pseudoquaternary $Mg_2Si_{1-x-y}Sn_xGe_y$-Based Materials

K. KUTORASINSKI,[1,3] J. TOBOLA,[1] S. KAPRZYK,[1] A.U. KHAN,[2] and TH. KYRATSI[2]

1.—Faculty of Physics and Applied Computer Science, AGH University of Science and Technology, 30-059 Krakow, Poland. 2.—Department of Mechanical and Manufacturing Engineering, University of Cyprus, 1678 Nicosia, Cyprus. 3.—e-mail: kutorasinski@fis.agh.edu.pl

A theoretical study is presented on complex pseudoternary Bi-doped $Mg_2Si_{1-x-y}Sn_xGe_y$ materials, which have recently been revealed to reach high thermoelectric figures of merit (ZT) of ~1.4. Morphological characterization by scanning electron microscopy and energy-dispersive x-ray spectroscopy indicated that the investigated samples were multiphase and that the alloy with nominal composition $Mg_2Si_{0.55}Sn_{0.4}Ge_{0.05}$ contained three phases: $Mg_2Si_{0.35}Sn_{0.6}Ge_{0.05}$ (Sn-rich phase), $Mg_2Si_{0.65}Sn_{0.3}Ge_{0.05}$ (Si-rich phase), and $Mg_2Si_{0.15}Sn_{0.5}Ge_{0.35}$ (Ge-rich phase). The electronic structure of all these phases was calculated in the framework of the fully charge self-consistent Korringa–Kohn–Rostoker method with the coherent potential approximation (KKR-CPA) to treat chemical disorder. Electron transport coefficients such as the electrical conductivity, thermopower, and the electronic part of the thermal conductivity were studied by combining the KKR-CPA technique with Boltzmann transport theory. The two-dimensional (2D) plots (as a function of electron carrier concentration and temperature), computed for the thermopower and power factor, well support the large thermoelectric efficiency detected experimentally. Finally, employing the experimental value of the lattice thermal conductivity as an adjustable parameter, it is shown that $ZT \approx 1.4$ can be reached for an optimized Bi content near $T \approx 900$ K in case of the nominal composition as well as the Sn-rich phase. The question of the effect of disorder on the convergence of the conduction bands and thus the electron transport properties is addressed through detailed examination of the Fermi surfaces.

Key words: Electronic structure, thermoelectric properties, Boltzmann transport, semiconductor doping

INTRODUCTION

$Mg_2Si_{1-x}Ge_x$, $Mg_2Si_{1-x}Sn_x$, $Mg_2Ge_{1-x}Sn_x$ alloys have attracted much attention as they are composed of cheap (except germanium), abundant, and environmentally friendly (nontoxic) raw materials. They also have a high figure of merit and the lowest density amongst all efficient thermoelectrics. $Mg_2Si_{1-x}Sn_x$ has been found to be the most favorable in terms of thermoelectric energy conversion, as it has the highest thermal resistivity due to the maximum mass difference between its components.[1–3] However, quasiternary solid solutions $Mg_2Si_{1-x-y}Sn_yGe_z$ have attracted much less attention. Very recently, a high figure of merit $ZT \approx 1.4$ was measured in the Bi-doped $Mg_2Si_{1-x-y}Sn_yGe_z$ system.[4] On the other hand, morphological characterization carried out by scanning electron microscopy and energy-dispersive x-ray spectroscopy (EDX) indicated that the main feature of typical micrographs obtained in backscatter mode was a

(Received October 30, 2013; accepted April 22, 2014; published online June 3, 2014)

mosaic-like texture.[4] EDX maps for the different elements, i.e., Mg, Si, Sn, and Ge, showed that the distributions of Mg, Si, Sn, and Ge are not homogeneous, since there are areas richer in Si or Sn, suggesting the appearance of phase separation. Ge-rich inclusions were also found. It appears that, for the nominal alloy compound $Mg_2Si_{0.55}Sn_{0.4}Ge_{0.05}:Bi_x$ with $x \approx 0.02$ that exhibited the largest ZT value, three phases were detected: an Sn-rich phase, i.e., $Mg_2Si_{0.35}Sn_{0.6}Ge_{0.05}$ (a = 6.598 Å), an Si-rich phase, i.e., $Mg_2Si_{0.65}Sn_{0.3}Ge_{0.05}$ (a = 6.475 Å), and a Ge-rich phase, i.e., $Mg_2Si_{0.15}Sn_{0.5}Ge_{0.35}$ (a = 6.569 Å), with different relative contributions. The aforementioned lattice parameters were determined from Vegard's law using the following values for the end-compounds: 6.351 Å for Mg_2Si, 6.763 Å for Mg_2Sn, and 6.386 Å for Mg_2Ge.

To investigate such a complex material from a theoretical point of view, we performed electronic structure calculations combined with Boltzmann transport modeling for four cases separately, i.e., for three alloy compositions close to the aforementioned phases and also for the nominal composition. The Korringa–Kohn–Rostoker (KKR)[5–8] method based on Green-function multiple scattering theory was used to compute the electronic band structure and kinetic parameters of electrons in the vicinity of the Fermi energy (E_F). The coherent potential approximation (CPA) was employed to account for chemical disorder effects (note that Si, Ge, Sn, and Bi occupy the same crystallographic site) on the electronic structure self-consistently. The linearized Boltzmann equation is implemented to determine electron transport coefficients such as the electrical conductivity σ [used to extract the electron lifetime from experimental $\sigma_{exp}(T)$], the Seebeck coefficient S, and the electronic part of the thermal conductivity κ_e. Quite recently, this procedure was successfully applied to n-type $Mg_2Si_{1-x}Sn_x$ thermoelectric material,[9] which has been intensively investigated[10–12] both experimentally and theoretically due to the so-called conduction-band convergence.[1,13–15] In this work, we extend such theoretical investigations to the very promising pseudoquaternary $Mg_2Si_{1-x-y}Sn_xGe_y:Bi$.

This paper is organized as follows. The next section presents theoretical details of the electron transport coefficient calculations in terms of transport functions. A constant relaxation time approximation is employed for the electron scattering mechanism. "Results and Discussion" section reports on the computational results for the temperature-dependent transport properties, i.e., $\sigma(T)$, $S(T)$, and $\kappa_e(T)$, in Bi-doped $Mg_2Si_{1-x-y}Sn_xGe_y$. This section also presents maps of the power factor $PF(n,T) = S^2\sigma$ and the figure of merit $ZT(n,T) = \sigma S^2/\kappa$ (with $\kappa = \kappa_e + \kappa_l$) versus electron concentration n and temperature T, assuming experimental values of the lattice thermal conductivity κ_l. The article ends with "Conclusion" section.

THEORETICAL AND COMPUTATIONAL DETAILS

Boltzmann transport theory was employed to calculate the electron transport properties. In this approach, transport quantities can be expressed in compact form as[16]

$$\begin{aligned} \boldsymbol{\sigma}_e &= \mathscr{L}^{(0)}, \\ \boldsymbol{S} &= -\frac{1}{eT}\frac{\mathscr{L}^{(1)}}{\mathscr{L}^{(0)}}, \\ \boldsymbol{\kappa}_e &= \frac{\mathscr{L}^{(2)}}{e^2T} - \frac{\mathscr{L}^{(1)}\mathscr{L}^{(1)}}{e^2T\mathscr{L}^{(0)}}, \end{aligned} \tag{1}$$

where

$$\mathscr{L}^{(\alpha)} = \int d\mathscr{E}\left(-\frac{\partial f}{\partial \mathscr{E}}\right)(\mathscr{E}-\mu)^{\alpha}\boldsymbol{\sigma}(\mathscr{E}). \tag{2}$$

The transport function $\sigma(\mathscr{E})$ is the key quantity in Boltzmann transport modeling, since together with the chemical potential μ, it contains all the material-related information. Generally, it is a tensor and has the form

$$\boldsymbol{\sigma}(\mathscr{E}) = e^2\sum_n \int \frac{\mathrm{d}\mathbf{k}}{4\pi^3}\tau_n(\mathbf{k})\mathbf{v}_n(\mathbf{k})\otimes\mathbf{v}_n(\mathbf{k})\delta(\mathscr{E}-\mathscr{E}_n(\mathbf{k})), \tag{3}$$

where $\otimes$ is the Kronecker product. The transport function contains two functions designating the electronic properties of the system, namely the band structure $\mathscr{E}_n(\mathbf{k})$ and the electron lifetime of bands $\tau_n(\mathbf{k})$,, which describe possible scattering processes. In standard density functional theory (DFT) calculations, it is impossible to take into account all these electron diffusion effects.[17–20] Fortunately, it has been shown[9,21,22] that assuming the function $\tau_n(\mathbf{k})$ to be a constant τ_0 (the constant lifetime approximation) often gives results in close agreement with experiment.

In practice, the k-space volume integration in Eq. 3 is replaced by surface integration:

$$\int \mathrm{d}\mathbf{k}\delta(\mathscr{E}-\mathscr{E}_n(\mathbf{k})) = \int\limits_{S(\mathscr{E})} \frac{\mathrm{dS}}{|\nabla_k\mathscr{E}_n(\mathbf{k})|}, \tag{4}$$

where the isoenergetic surfaces $S(\mathscr{E})$ are calculated using a marching cube algorithm[23] on a three-dimensional (3D) mesh. In this work, the Brillouin zone was inscribed into a box divided into 512,000 voxels (80 × 80 × 80). Using Eq. 4 and the regular structure relation $|\mathbf{v}\otimes\mathbf{v}| = 1/3\mathbf{v}^2$, the transport function can be represented as

$$\sigma_\tau(\mathscr{E}) = \tau_0\frac{e^2}{\hbar}\sum_n \int\limits_{S_n(\mathscr{E})} \frac{dS}{4\pi^3}\mathbf{v}(S_n(\mathscr{E})). \tag{5}$$

In general, the chemical potential μ is calculated from the density of states (DOS) function. Next,

employing a rigid-band model,[24] the effect of doping can be simulated by adding extra carriers n into the semiconducting system

$$n_0 + n = \int d\mathscr{E} g(\mathscr{E}) \frac{1}{1 + e^{\frac{\mathscr{E}-\mu(T,n_d)}{k_B T}}}, \quad (6)$$

where n_0 corresponds to the number of electrons filling the valence bands. In the case of the Bi-doped system, our analysis was based on the KKR-CPA electronic band structure calculated for $Mg_2Si_{1-x-y}Sn_xGe_y$ with 2% of Bi diluted on the Si/Ge/Sn site, and the Fermi level was found above the conduction-band edge. To investigate different magnitudes of doping, E_F was varied along these electronic bands to mimic carrier concentrations in the range $10^{19}\,\mathrm{cm}^{-3} < n < 10^{21}\,\mathrm{cm}^{-3}$.

The lifetime τ_0 used in this work was calculated by matching the experimental and calculated conductivity

$$\sigma_{\mathrm{exp}}(T) = \tau_0(T)\frac{1}{3}\frac{e^2}{\hbar}\int \mathrm{d}\mathscr{E}\left(-\frac{\partial f}{\partial \mathscr{E}}\right)\sum_n \times \int_{S_n(\mathscr{E})} \frac{\mathrm{dS}}{4\pi^3}|\mathbf{v}(S_n(\mathscr{E}))|. \quad (7)$$

This matching was done using the experimental conductivity for the sample with 2% Bi and calculated for four different compositions, separately (for all temperatures independently). This yielded four different $\tau_0(T)$ relations with an almost linear dependence on temperature; therefore only two values, corresponding to T = 300 K and T = 800 K, are presented in Table I.

RESULTS AND DISCUSSION

It is worth noting that the electrical conductivity and thermopower measured for the multiphase samples with different Bi contents show that the $\sigma(T)$ and $S(T)$ curves no longer change when the Bi concentration exceeds 2% (likely indicating the solubility limit for this dopant).

Figure 1 shows that a difference in the Seebeck coefficient is visible only for the sample with 1% nominal Bi content, whereas the samples with higher Bi concentrations, namely 1.75%, 2%, and 2.5%, exhibit very similar $S(T)$ dependences. Consequently, the experimental thermopower for these three Bi contents fits the theoretical $S(T)$ curve for $n \approx 2.5 \times 10^{20}\,\mathrm{cm}^{-3}$, which corresponds to 1.8% nominal Bi content. Figure 2 indicates that the measured electrical conductivity increases with Bi content up to 2%. There is no difference between the samples with 2% and 2.75% Bi concentration. The above-mentioned differences in the experimental behaviors of the thermopower and electrical conductivity with Bi content suggest different solubility limits of Bi in different phases.

KKR-CPA calculations resulted in an energy gap between valence and conduction bands in all considered phases. However, as expected from the local density approximation (LDA) employed in this work, such computations tend to underestimate bandgap values. To enable reliable analysis of temperature-dependent electron transport parameters, the calculated gap was then broadened to the experimental value.[25]

Electronic structure calculations of Mg_2(Si-Sn-Ge) show that the important differences among the results obtained for the three considered phases

Table I. Electron lifetime (in 10^{-15} s) as a function of temperature for different phases used in this work

Composition	τ_0 (300 K)	τ_0 (800 K)
Sn-rich phase (ph 1) $Mg_2Si_{0.27}Sn_{0.66}Ge_{0.05}Bi_{0.02}$	7.1	3.6
Si-rich phase (ph 2) $Mg_2Si_{0.67}Sn_{0.26}Ge_{0.05}Bi_{0.02}$	8.3	4.0
Ge-rich phase (ph 3) $Mg_2Si_{0.14}Sn_{0.49}Ge_{0.35}Bi_{0.02}$	7.9	3.9
Nominal phase (ph N) $Mg_2Si_{0.53}Sn_{0.4}Ge_{0.05}Bi_{0.02}$	7.4	3.8

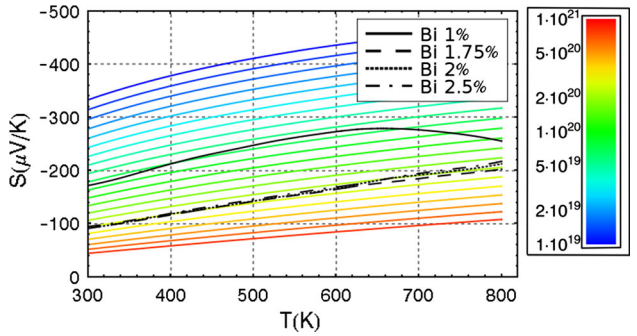

Fig. 1. Experimental thermopower as a function of temperature for multiphase samples with different Bi contents (black lines). Calculated thermopower for different carrier concentrations is plotted with different color lines (see legend) (Color figure online).

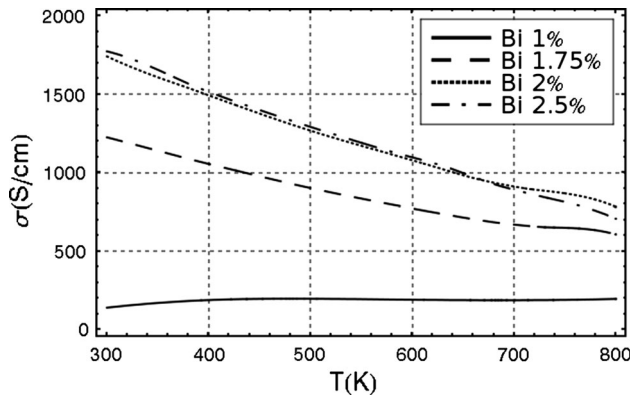

Fig. 2. Experimental electrical conductivity versus temperature in multiphase samples with different Bi contents.

(also compared with the nominal composition) essentially concern the two lowest-lying conduction bands. Inspecting the dispersion curves for high-symmetry directions in more detail, it appears that the relative position of the two conduction bands near the X point is mostly affected by the alloy composition. One can tentatively connect the mutual shift of these bands with the variable lattice parameter. These electronic structure features are best illustrated in Fig. 3. It can be noticed that the Sn-rich and nominal phases exhibit the smallest energy separation between the two conduction bands (near the X point). Therefore, as already shown[9] for the $Mg_2(Si\text{-}Sn)$ system, this electronic structure behavior presumably enhances the thermoelectric properties of these alloys. When these two bands tend to converge near the X point (the band separation almost vanishes for phases ph 1 and ph N, as shown in Fig. 3), the thermopower indeed reaches its highest values (Fig. 4a) among the considered phases. The influence of the conduction band separation on the Seebeck coefficient is best seen at lower temperature and lower carrier concentration (in particular below $3 \times 10^{20}\,\mathrm{cm}^{-3}$). As a consequence, these electronic band features have an effect on the power factor (Fig. 5). For 2% Bi content and at temperature of 900 K, the power factor reaches a value about 15% higher for phase ph N (or ph 1) with respect to the worst one (ph 2), which exhibits the largest conduction band separation near the X point.

To estimate the dimensionless figure of merit ZT in these four phases, the lattice part of the thermal conductivity (κ_l) was estimated from experimental data.[4] Accordingly, κ_l was chosen to decrease linearly with temperature from a value of $\kappa_l = 2.0\,\mathrm{W\,m^{-1}K^{-1}}$ at 300 K to $\kappa_l = 1.25\,\mathrm{W\,m^{-1}K^{-1}}$ at 800 K. Besides, the thermal conductivity was taken to be the same for all investigated compounds, allowing coherent comparison among the results obtained for the four phases, to focus on the contribution of the electronic quantities to ZT. The resulting ZT maps depending on the carrier concentration and temperature are presented in Fig. 6. It can be noticed that the highest ZT values were found for $n \approx 1.5 \times 10^{20}\,\mathrm{cm}^{-3}$ (corresponding to ca. 1% Bi) and $T \approx 900\,\mathrm{K}$ for the Sn-rich or nominal

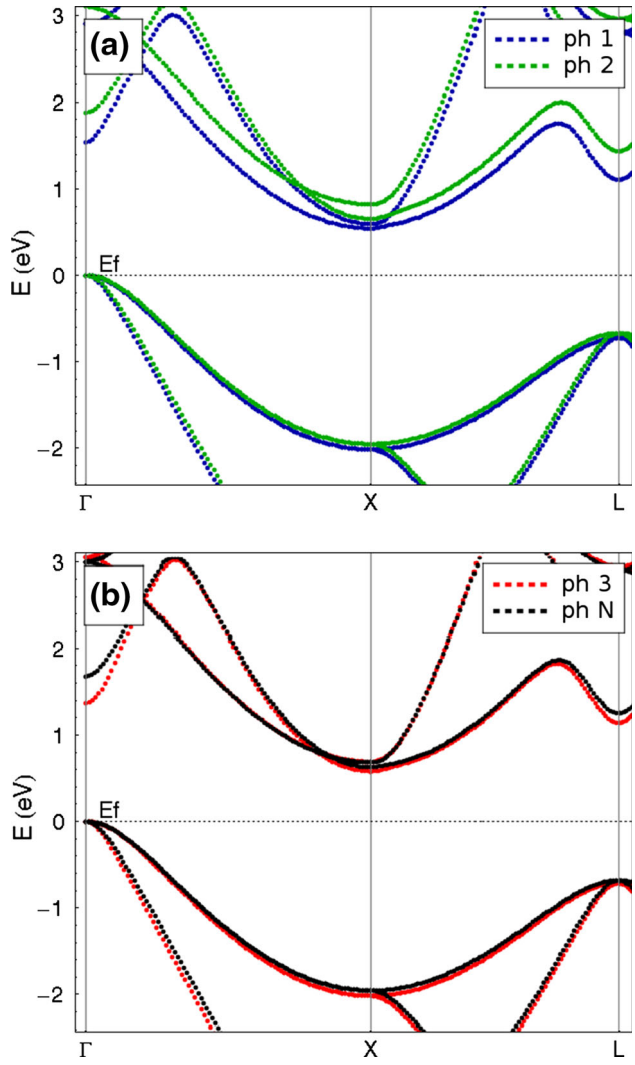

Fig. 3. Electronic band structure near X point for: (a) Si-rich and Sn-rich phases, and (b) nominal and Ge-rich phases. Alloy compositions are listed in Table I. The horizontal line marks the top of the valence bands (Color figure online).

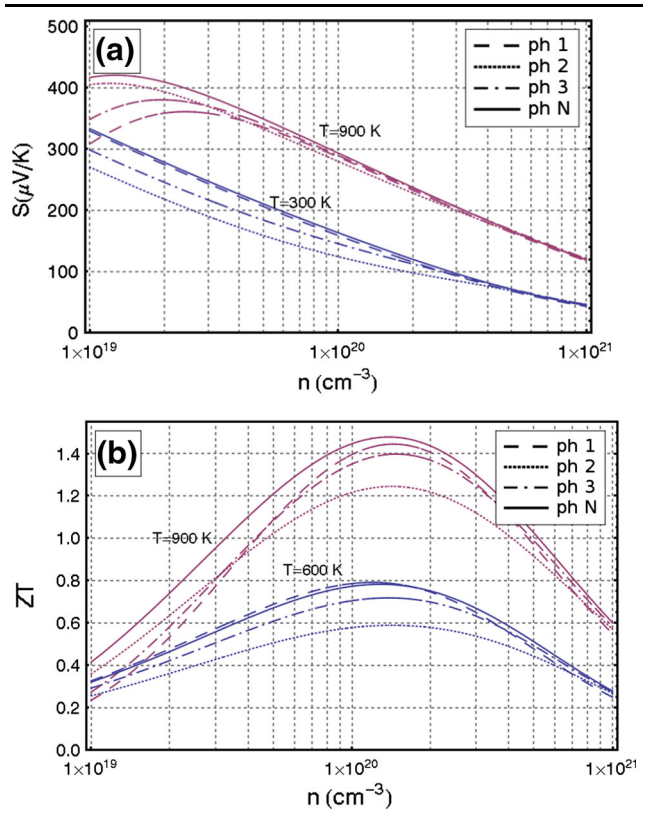

Fig. 4. (a) Thermopower and (b) ZT versus the logarithm of concentration at different temperatures for the four different phases (see Table I for exact alloy compositions) (Color figure online).

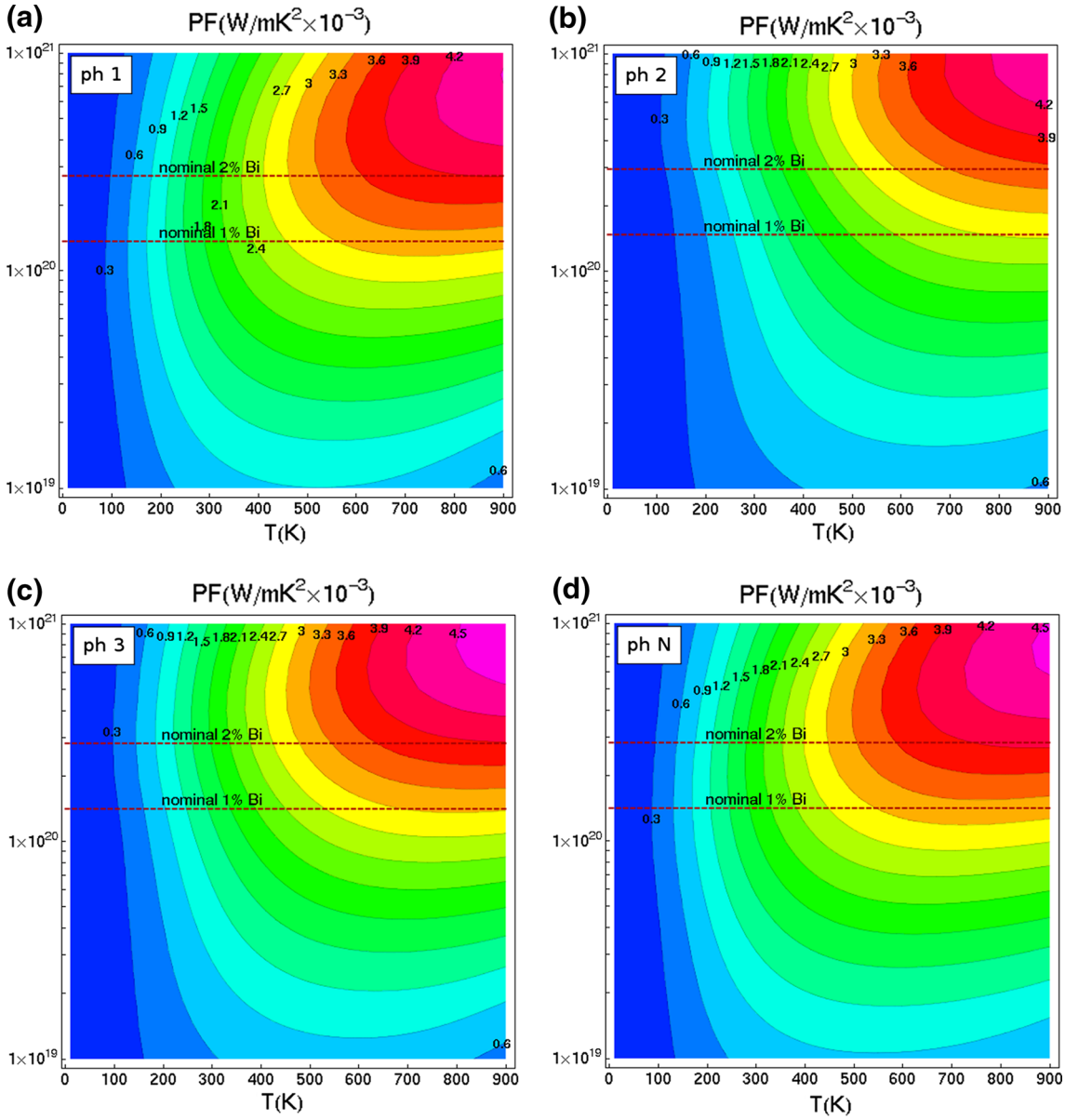

Fig. 5. Power factor as a function of concentration and temperature for the considered alloy compositions: (a) Sn-rich phase, (b) Si-rich phase, (c) Ge-rich phase, and (d) nominal phase. Alloy compositions are listed in Table I. Dashed horizontal lines mark nominal Bi concentrations of 1% and 2% (Color figure online).

phases, in line with the results obtained for the power factor (Fig. 5). As mentioned above, the Si-rich phase, which exhibits large splitting between the two conduction bands (Fig. 3, top), also has the worst ZT among the four presented alloy compositions (Fig. 4b).

CONCLUSIONS

We have shown that the KKR-CPA method combined with the Boltzmann transport approach can be successfully adopted for theoretical study of thermoelectric properties in the complex pseudoternary n-type $Mg_2Si_{1-x-y}Sn_xGe_y$ system, which contains a high degree of chemical disorder (alloying and doping). The implemented procedure (within the constant relaxation time approximation) satisfactorily reproduces the dependence of electron transport properties, such as the thermopower and power factor, on temperature and carrier concentration. It has been found that the high efficiency of thermoelectric conversion measured in Bi-doped nominal $Mg_2Si_{0.53}Sn_{0.4}Ge_{0.05}$, which actually consists of three phases: $Mg_2Si_{0.35}Sn_{0.6}Ge_{0.05}$ (Sn-rich phase), $Mg_2Si_{0.65}Sn_{0.3}Ge_{0.05}$ (Si-rich phase), and $Mg_2Si_{0.15}Sn_{0.5}Ge_{0.35}$ (Ge-rich phase), is likely due to the fact that two of them (ph 1 and ph N) exhibit similar thermoelectric parameters in the high temperature range. The ZT values versus temperature and carrier concentration were estimated using the

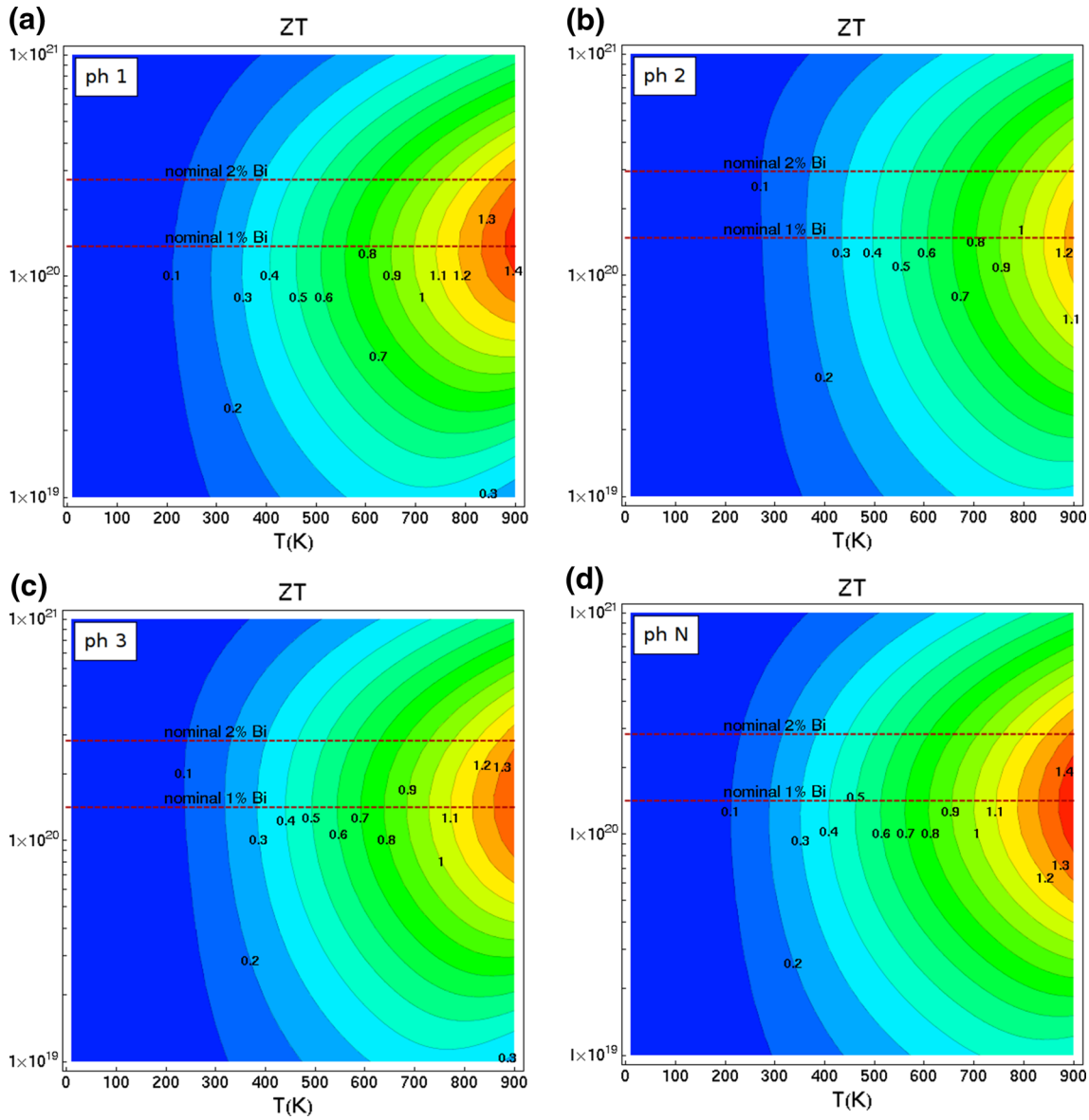

Fig. 6. *ZT* as a function of concentration and temperature for the considered alloy compositions: (a) Sn-rich phase, (b) Si-rich phase, (c) Ge-rich phase, and (d) nominal phase. Alloy compositions are listed in Table I. Dashed horizontal lines mark nominal Bi concentrations of 1% and 2% (Color figure online).

lattice part of the thermal conductivity as an adjustable parameter. $ZT = 1.4$ was achieved near 900 K at the experimental value of κ_l. It has also been shown that the Bi dopant presumably reaches its solubility limit close to 2%, preventing the achievement of the best working concentration.

ACKNOWLEDGEMENTS

The work was partially supported by the Polish National Science Center (NCN, Grant No. DEC-2011/02/A/ST3/00124 and UMO-2011/03/N/ST3/02644) and the Thermomag Project (FP7-NMP4-SL-2011-263207) cofunded by the European Space Agency and by individual partner organizations.

OPEN ACCESS

REFERENCES

1. V.K. Zaitsev, M.J. Fedorov, E.A. Gurieva, I.S. Eremin, P.P. Konstantinov, A.Y. Samunin, and M.V. Vedernikov, *Phys. Rev. B***74**, 045207 (2006).
2. X. Zhang, H. Liu, Q. Lu, J. Zhang, and F. Zhang, *Appl. Phys. Lett.***103**, 063901 (2013).

3. W. Liu, Q. Zhang, K. Yin, H. Chi, X. Zhou, X. Tang, and C. Uher, *J. Solid State Chem.***203**, 333 (2013).
4. A.U. Khan, N. Vlachos, and Th. Kyratsi, *Scr. Mater.***69**, 606 (2013).
5. J.S. Faulkner and G.M. Stocks, *Phys. Rev. B***21**, 3222 (1980).
6. S. Kaprzyk and A. Bansil, *Phys. Rev. B***42**, 7358 (1990).
7. A. Bansil, S. Kaprzyk, P.E. Mijnarends, and J. Tobola, *Phys. Rev. B***60**, 13396 (1999).
8. T. Stopa, S. Kaprzyk, and J. Tobola, *J. Phys. Condens. Matter***16**, 4921 (2004).
9. K. Kutorasinski, J. Tobola, and S. Kaprzyk, *Phys. Rev. B***87**, 195205 (2013).
10. W. Liu, X. Tang, and J. Sharp, *J. Phys. D Appl. Phys.***43**, 085406 (2010).
11. P. Zwolenski, J. Tobola, and S. Kaprzyk, *J. Electron. Mater.***40**, 889 (2011).
12. W.H. Fan, R.X. Chen, L.Q. Wang, P.D. Han, and Q.S. Meng, *J. Electron. Mater.***40**, 1209 (2011).
13. W. Liu, X. Tan, K. Yin, H. Liu, X. Tang, J. Shi, Q. Zhang, and C. Uher, *Phys. Rev. Lett.***108**, 166601 (2012).
14. J. Tobola, S. Kaprzyk, and H. Scherrer, *J. Electron. Mater.***39**, 2064 (2010).
15. X.J. Tan, W. Liu, H.J. Liu, J. Shi, X.F. Tang, and C. Uher, *Phys. Rev. B***85**, 205212 (2012).
16. N.W. Ashcroft and N.D. Mermin, *Solid State Physics* (Philadelphia: Saunders, 1976).
17. I. Mertig, *Rep. Prog. Phys.***62**, 237 (1999).
18. S. Ahmad and S.D. Mahanti, *Phys. Rev. B***81**, 165203 (2010).
19. W.H. Butler and G. Stocks, *Phys. Rev. B***29**, 4217 (1990).
20. T. Stopa, J. Tobola, S. Kaprzyk, E.K. Hlil, and D. Fruchart, *J. Phys. Condens. Matter***19**, 6379 (2006).
21. L. Chaput, G. Hug, P. Pécheur, and H. Scherrer, *Phys. Rev. B***71**, 121104(R) (2005).
22. L. Chaput, P. Pécheur, J. Tobola, and H. Scherrer, *Phys. Rev. B***72**, 085126 (2005).
23. W.E. Lorensen, *Comput. Graph.***21**, 163 (1987).
24. G. Goran, *Phys. Condens. Mater.***14**, 101 (1972).
25. V.K. Zaitsev, M.I. Fedorov, I.S. Eremin, and E.A. Gurieva, *Thermoelectrics Handbook: Macro to Nano*, ed. D.M. Rowe (Boca Raton: Taylor and Francis, 2006).